ACS OMEGA

http://pubs.acs.org/journal/acsodf

Article

Hydrogen Bonds and n → π* Interactions in the Acetylation of Propranolol Catalyzed by *Candida antarctica* Lipase B: A QTAIM Study

David A. Rincón, Markus Doerr,* and Martha C. Daza

Cite This: *ACS Omega* 2021, 6, 20992−21004

Read Online

ACCESS | Metrics & More | Article Recommendations | Supporting Information

ABSTRACT: Enzyme−substrate interactions play a crucial role in enzymatic catalysis. Quantum theory of atoms in molecules (QTAIM) calculations are extremely useful in computational studies of these interactions because they provide very detailed information about the strengths and types of molecular interactions. QTAIM also provides information about the intramolecular changes that occur in the catalytic reaction. Here, we analyze the enzyme−substrate interactions and the topological properties of the electron density in the enantioselective step of the acylation of (*R*,*S*)-propranolol, an aminoalcohol with therapeutic applications, catalyzed by *Candida antarctica* lipase B. Eight reaction paths (four for each enantiomer) are investigated and the energies, atomic charges, hydrogen bonds, and n → π* interactions of propranolol, the catalytic triad (composed of D187, H224, and S105), and the oxyanion hole are analyzed. It is found that D187 acts as an electron density reservoir for H224, and H224 acts as an electron density reservoir for the active site of the protein. It releases electron density when the tetrahedral intermediate is formed from the Michaelis complex and receives it when the enzyme−product complex is formed. Hydrogen bonds can be grouped into noncovalent and covalent hydrogen bonds. The latter are stronger and more important for the reaction than the former. We also found weak n → π* interactions, which are characterized by QTAIM and the natural bond orbital (NBO) analysis.

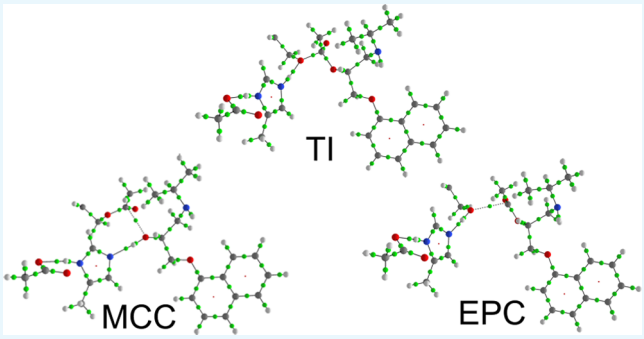

INTRODUCTION

β-Amino alcohols are present in many biologically active natural products and chiral auxiliaries containing common intermediates.[1−4] They play an increasingly important role in medicinal chemistry, pharmaceuticals, and in organic synthesis.[4−6] Some β-adrenergic blocking agents (β-blockers) are β-amino alcohols and are used in the treatment of a wide variety of human disorders like hypertension, sympathetic nervous system, heart failure, and cardiac arrhythmia[4,7,8] and also as insecticidal agents.[4,9] Compounds such as propranolol, 1-(1-methylethylamino)-3-(1-naphthoxy)-2-propanol, are β-adrenergic antagonists.[10] Propranolol is used to treat cardiovascular disorders[11−13] and is found as a racemic mixture.[14] In medical treatments, the *S*-enantiomer is preferred over *R*- because the *R*-enantiomer causes undesirable symptoms such as bronchoconstriction and diabetes.[15−17] Currently, researchers are seeking for different methodologies to obtain the preferred enantiomeric compound. Among them are techniques such as thin-layer chromatography with impregnated layers to separate the racemic mixture of propranolol,[18−20] enantioselective synthetic pathways,[21−24] or kinetic resolution of racemic propranolol by lipase-immobilized catalysis.[25−27]

Hydrolases are a group of enzymes whose function is to catalyze the reaction between any alcohol, amine, or ester and the acetyl functional group to produce an ester.[28−33] They also catalyze the inverse reaction from any ester, amide, or thioester to produce their synthons.[34−36] Hydrolases have also been implemented in industrial applications.[37,38] These enzymes do not lose their biological function at elevated temperatures and pressures. Also, the biological activity of these enzymes is retained when they are immersed in different organic solvents.[37]

One frequently used hydrolase is *Candida antarctica* lipase B, CalB.[39] The catalytic site of this enzyme consists of two components. The catalytic triad and the oxyanion hole. The former part is made up of aspartate, histidine, and serine (D187, H224, and S105), while the latter is composed of glutamine and threonine (Q106 and T40). The reaction

Received: May 16, 2021
Accepted: July 22, 2021
Published: August 3, 2021

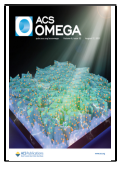

mechanism occurs in two steps: (i) acetylation of the enzyme and (ii) deacetylation of the enzyme. In the first step, an acetyl group is transferred to the hydroxyl group of S105. In the second step, the acetyl enzyme reacts with a nucleophile such as water, alcohols, amines, or peroxides to produce the ester compound, and S105 is recovered.[14,40] The acetylation of propranolol by lipase has been studied previously in our group. It was found that the enzyme acetylates only the propranolol hydroxyl group[41] and preferably reacts with the *R*-enantiomer.[14,42] In those studies, the focus was on the reaction and activation energies and on structural changes along the reaction. In the present work, our aim is to analyze the electronic structure and topological bonding along the reaction path to gain deeper insight into the interactions between the protein and substrate.

Quantum theory of atoms in molecules (QTAIM) allows us to analyze a characteristic of many-electron systems, the electron density, $\rho(\mathbf{r}_c)$. The bound atoms in a chemical system at the stationary point on the potential energy surface (PES) are considered as a set of nucleus-centered fragments, so-called atomic basins, Ω, that are separated by surfaces of zero-flux of the gradient of the electron density, $\nabla^2\rho(\mathbf{r}_c)$. The bonding between such atoms is associated with the network of lines of maximal density, the bond paths. Each of them consists of two density-gradient lines, which originate from the saddle critical points between atoms, where $\nabla^2\rho(\mathbf{r}_c) = 0$, and finish on the corresponding nuclei. The existence of bond critical points (BCP) on an interatomic line in a system at equilibrium is considered as a necessary and sufficient sign of a bonding interaction between the corresponding pair of atoms.[43−45]

The classification of bonds[46,47] is one application of QTAIM. Bader in his theory[44] proposed to distinguish between two kinds of chemical bonds: the shared shell (SS) and the closed shell interactions based on $\rho(\mathbf{r}_c)$ and $\nabla^2\rho(\mathbf{r}_c)$. The first type of bonds is usually associated with covalent bonds, and examples of the second type are the ionic and the hydrogen bond (HB).[48,49] Another QTAIM application is the analysis of molecular interactions between proteins and ligands.[50−53] These studies show the importance of HBs on the stabilization of ligands inside a protein active site. Another example of an interaction is the n → π^* interaction. In this interaction, the lone pair of electrons of an electronegative atom is delocalized over the antibonding π orbital (π^*) of an electron deficient π-system.[54−57]

Because the aim of this paper is to apply QTAIM to analyze the interactions between propranolol and the enzyme, all atoms involved in these interactions are part of the quantum mechanics (QM) region. In our previous study, the aminoacids of the oxyanion hole were not part of the QM region. Therefore, we expand the QM region to include aminoacids of the oxyanion hole. Our paper is structured as follows: First, we analyze the effect of this expansion on the energy profiles. Then, an analysis of the atomic charges and topological properties of interactions involved in the reaction mechanism is presented. Finally, the role of n → π^* interactions on the enzymatic kinetic resolution of propranolol by CalB is analyzed.

METHODS

The starting structures for all molecular configurations studied in the present paper were taken from our previous work.[14] Here, we only give a short description of the procedure, for details see ref. 14. The coordinates of lipase B from *C. antarctica* were taken from the crystal structure (Protein Data Bank (PDB) ID: 1TCA).[58] The protonation states of titratable residues were assigned using the PROPKA module of PDB2PQR.[59−63] Furthermore, the orientations of all side chains were arranged such that the hydrogen bond network is optimized. After proper assignment of the protonation states, the hydroxyl group of the S105 side chain was replaced by acetate to obtain the acetyl enzyme (AcetylCalB). The acetate oxygen was positioned to form hydrogen bonds with the residues of the oxyanion hole. All crystal waters were retained. Using this structure, MD simulations in an explicit toluene solvent were performed.

To build starting structures for the tetrahedral intermediate (TI), the dominant structure of AcetylCalB during the MD simulation was used as a target for manual covalent docking of (*R*)- and (*S*)-propranolol. Six starting structures with distinct conformations were created by varying the torsion angles of propranolol in its TI form. The TI structures were then subjected to postdocking optimization.[64] The optimized structures were further subjected to 1.5 ns MD simulations in explicit toluene. Representative snapshots of the TI taken from the MD simulations served as starting points for the subsequent QM/molecular mechanics (MM) calculations using B3LYP[65−68] /TZVP[69] for the QM region, consisted of the catalytic triad (D187, H224, and S105) and propranolol, and the CHARMM force field for the MM region. The QM region in these calculations consisted of propranolol and the catalytic triad. After optimization of the structure of the TI, structures of the Michaelis complex (MCC) and enzyme−product complex (EPC) were obtained by performing relaxed PES scans, followed by geometry optimization.

In the present study, the QM region is formed by the catalytic triad, the oxyanion hole (Q106 and T40), and propranolol. The expansion of the QM region made it necessary to reoptimize the structures, as described below. The rest of the system, the MM region, was treated classically, using a force field. The total charge of the QM region was −1. All atoms within 7 Å of the QM region, the active region, were unconstrained during QM/MM optimization, whereas the positions of the more distant atoms were kept fixed.

The chosen QM/MM methodology is similar to that used in our previous study.[14] The QM/MM calculations were performed with the ORCA quantum chemistry program package.[70−72] Electrostatic interactions between the QM region and the surrounding point charges of the MM region were treated using an electrostatic embedding scheme with charge shift correction.[73,74] Valences at the covalent bonds crossing the QM/MM boundary were saturated using hydrogen link atoms.[75] Density functional theory was used to describe the QM region, while for the MM region, the CHARMM36 force field was employed.[76]

The initial geometries were preoptimized in Cartesian coordinates using the semiempirical tight-binding method XTB2.[77−82] Then, the optimized geometries were again optimized with the B97-3c[83] functional with the TZVP[69] basis set. These structures were then further refined using the B3LYP[65−68] functional with the same basis set. Finally, an optimization in internal coordinates was performed, using the same functional and basis set. On these minimized geometries, a single point calculation was done to obtain the wave function file to be analyzed into the QTAIM framework.

All computed reaction profiles involve three stationary points: the acetylated CalB propranolol Michaelis complex

https://doi.org/10.1021/acsomega.1c02559
ACS Omega 2021, 6, 20992−21004

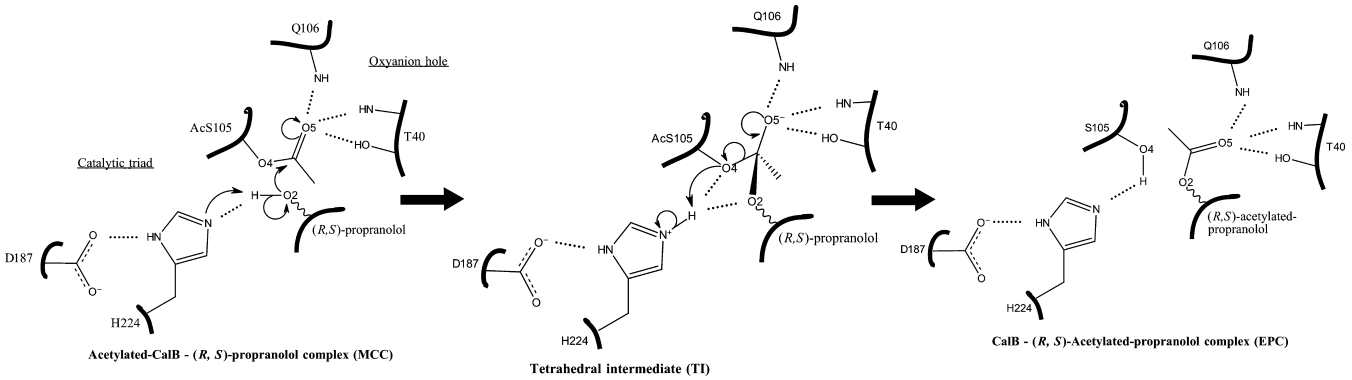

Figure 1. Mechanism of the reaction of the deacetylation step. Dashed lines represent HBs.

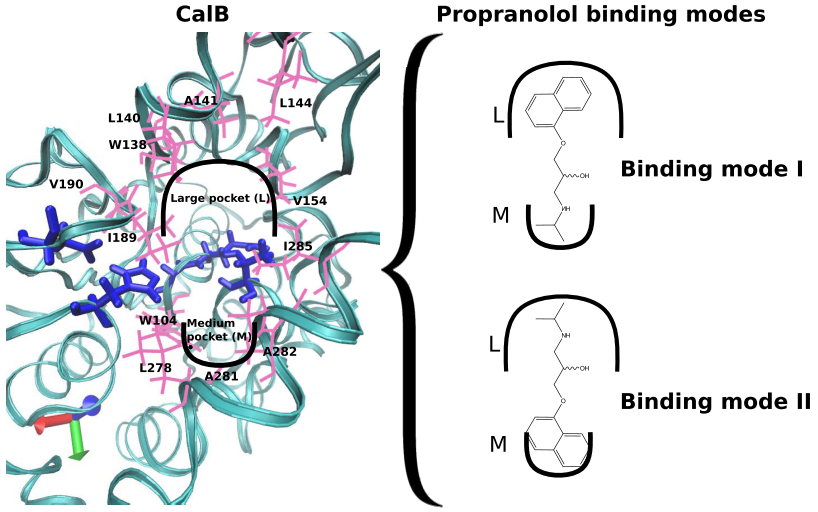

Figure 2. Schematic view of the binding modes of propranolol in the active site of CalB. Left: The main residues comprising the walls of the large and medium size pockets of CalB are shown in pink. The catalytic triad and the residues of the oxyanion hole are shown in blue. This figure is adapted from ref 14.

(MCC), the tetrahedral intermediate (TI), and the CalB acetylated propranolol enzyme−product complex (EPC). Unless mentioned otherwise, all energies reported in this paper are given with respect to the energy of the MCC.

The QTAIM analysis of the electron density $\rho(\mathbf{r}_c)$ for all systems was carried out with the AIMALL software.[84] This analysis allows obtaining the atomic basins and their corresponding properties, such as the atomic charge, $q(\Omega)$, and atomic energy, $E(\Omega)$. In this paper, the atomic charges were analyzed within the QTAIM framework. Also, topological properties at bond critical points, BCP, such as the electron density, $\rho(\mathbf{r}_c)$, Laplacian of the electron density, $\nabla^2\rho(\mathbf{r}_c)$, local potential energy density, $V(\mathbf{r}_c)$, local kinetic energy density, $G(\mathbf{r}_c)$, and local energy density, $H(\mathbf{r}_c)$ were analyzed. This last topological property is obtained from the Cremer and Kraka relationship.[85]

Hayashi et al.[47] introduced a procedure to classify bonds based on the Cremer−Kraka relationship:[85]

$$H(\mathbf{r}_c) = V(\mathbf{r}_c) + G(\mathbf{r}_c) \quad (1)$$

$$(\hbar^2/8m)\nabla^2\rho(\mathbf{r}_c) = H(\mathbf{r}_c) - V(\mathbf{r}_c)/2 \quad (2)$$

Their analysis is based on eqs 1 and 2, where the first equation relates the local potential energy density, $V(\mathbf{r}_c)$, with the local kinetic energy density, $G(\mathbf{r}_c)$, to obtain the local energy density, $H(\mathbf{r}_c)$. The second equation relates the Laplacian $\nabla^2\rho(\mathbf{r}_c)$ with the local potential and total energy densities. Based on these relationships, bonds are classified based on $H(\mathbf{r}_c)$ and $\nabla^2\rho(\mathbf{r}_c)$. This classification is described in Scheme S1 of the Supporting Information, SI. To better understand the n → π^* interactions, the natural bond orbital (NBO) analysis was performed, using NBO 7.0.[86] Molecular visualization was rendered using Visual Molecular Dynamics[87] and AIMStudio from AIMALL.

RESULTS AND DISCUSSION

The naming scheme employed for all structures in this paper is reported in Figures S1−S7. The acetylation of propranolol starts with the formation of MCC, where the OH group of propranolol is located near to the acetylated serine, AcS105. In this complex, a HB is formed between the OH group of propranolol and Nπ of H224. The next step consists of a nucleophilic attack of the OH group of propranolol on the carbonyl group of the acetylated serine, forming the tetrahedral intermediate, and transferring the proton to H224. The protonation of histidine is also an essential step in the reaction mechanism of proteases, which have the same catalytic triad as lipases, and it is generally accepted that histidine is not protonated in the MCC but protonated in the tetrahedral intermediate (TI).[88−93] The TI is stabilized by HBs with T40

https://doi.org/10.1021/acsomega.1c02559
ACS Omega 2021, 6, 20992−21004

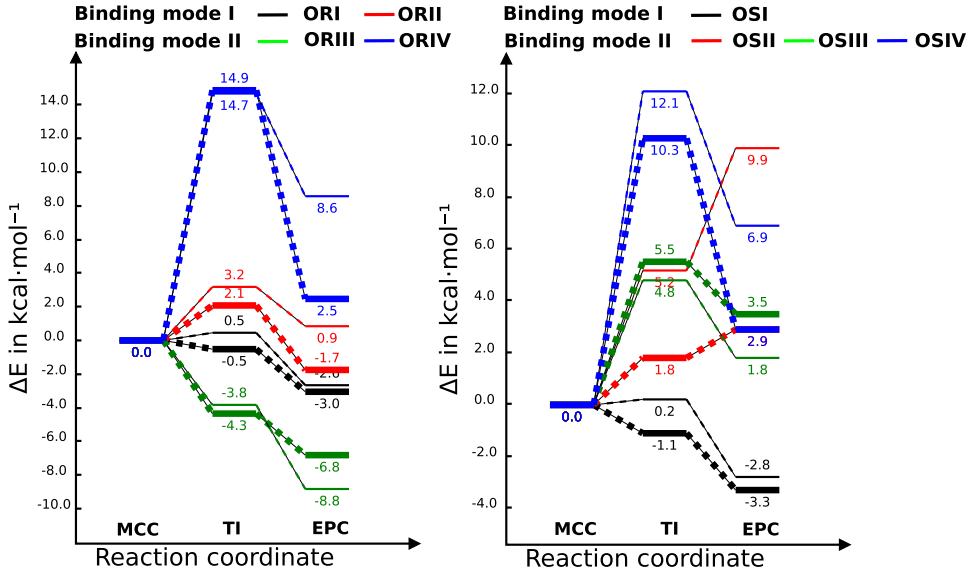

Figure 3. QM(B3LYP/TZVP)/MM energy profiles for the conversion of (*R*)- (left) and (*S*)-propranolol (right) to O-acetylated propranolol in binding modes I and II. Energies are given relative to the MCC. Thin lines correspond to values obtained in ref 14. Thick lines are values obtained in the present study.

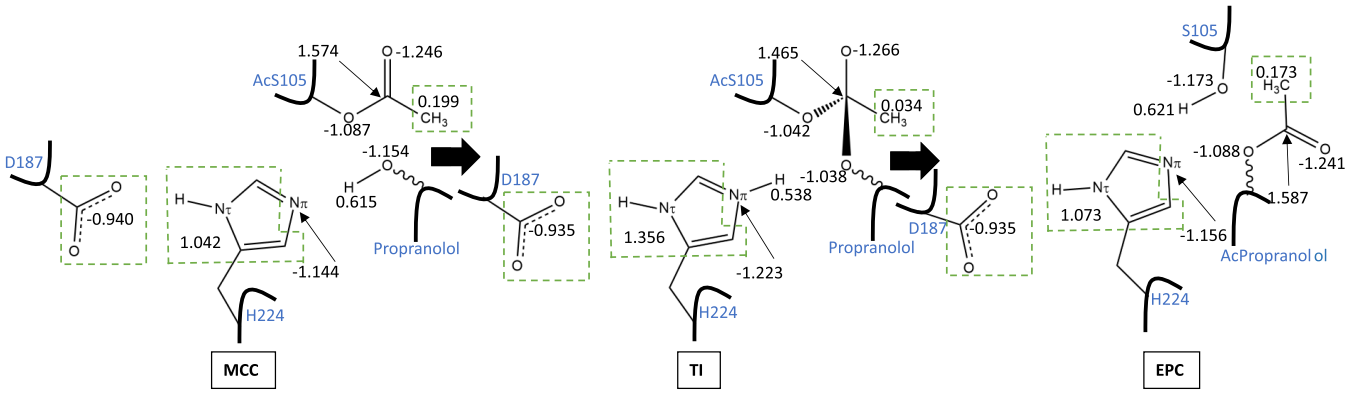

Figure 4. Atomic charges (in au, averaged over all reaction paths) of aminoacidic residues and atoms of the MCC, TI, and the EPC. Dashed lines indicate groups of atoms with their corresponding charges.

and Q106. Finally, the proton is transferred from the protonated H224 to S105 and the acetylated propranolol is formed. The mechanism and the relevant interactions are shown in Figure 1.

Moreover, the active site of CalB is composed of two pockets: one large and the other of medium size (Figure 2). The large pocket is located above the catalytic triad, and the medium size pocket is below it. In a previous investigation,[14] it was found that propranolol accommodates inside the active site in two binding modes for each propranolol isomer. In binding mode I, the naphthoxy group of propranolol is oriented toward the large pocket and the isopropylamine side chain is in the medium size pocket. In binding mode II, the orientation of propranolol is upside down compared with the previous binding mode (Figure 2).

In reaction paths ORI and ORII, (*R*)-propranolol is oriented in binding mode I, and in ORIII and ORIV, in binding mode II. In reaction path OSI, (*S*)-propranolol binds in binding mode I, while in the other three reaction paths, it binds in binding mode II.

The predominant interactions between propranolol and the active site of CalB are hydrogen bonds (Figure 1).

Energy Profiles. Figure 3 shows the energy profiles obtained in the previous study and those obtained in the present study. OR and OS configurations are shown in Figures S9−S32. The relative energies for the eight energy profiles obtained in the previous study are similar to those obtained in the present study, except for ORIV, OSII, and OSIV. In the EPC of ORIV, the orientation of the carbonyl group in the oxyanion hole is different after reoptimization, resulting in an elongation of the hydrogen bond with the NH group by 1.75 Å and of the hydrogen bond with the OH group of T40 by 0.8 Å (Figure S20). The energy differences observed in the TI of OSII are caused by many relatively small conformational changes in the MM region (Figures S25 and S33). In the EPC of OSII, large differences in the conformation of propranolol can be observed. The acceptor atom of the intramolecular hydrogen bond of the NH group changes from O2 to O1c, resulting in a relatively small overall change of the QM energy. The largest energy differences are due to structural differences in the MM region (Figures S26 and S33). In the EPC of OSIV, the orientation of propranolol in the active site changes somewhat, resulting in changes of the QM energy by 2.6 kcal/mol, accompanied by smaller changes of the MM energy by 1.5

https://doi.org/10.1021/acsomega.1c02559
ACS Omega 2021, 6, 20992−21004

Table 1. Sum of the Charges and Charge Differences (in au, Averaged over All Reaction Paths) for the Aminoacidic Residues of the Active Site of CalB and Propranolol

aminoacidic residues	MCC	TI	EPC	Δq (TI − MCC)	Δq (EPC − TI)
D187	−0.914	−0.880	−0.902	0.034	−0.022
H224	0.046	0.858	0.065	0.812	−0.793
AcS105	−0.062	−0.398		−0.335	
S105		−0.094	−0.129		−0.035
Q106	−0.333	−0.326	−0.342	0.007	−0.016
T40	−0.042	−0.055	−0.040	−0.014	0.016
propranolol	−0.032	−0.520		−0.488	
acetylated propranolol		−0.285	0.023		0.308

Table 2. Ranges of Distances and QTAIM Properties (in au) of Covalent Bonds (SS), Covalent HBs (rCS), and Ionic HBs (pCS) Found in All Reaction Paths

type of bond	limits	d (Å)	$\rho(\mathbf{r}_c)$	$\nabla^2\rho(\mathbf{r}_c)$	$H(\mathbf{r}_c)$
SS	min.	0.973	250.2×10^{-3}	-2360.1×10^{-3}	-767.6×10^{-3}
	max.	1.559	420.0×10^{-3}	-307.5×10^{-3}	-180.7×10^{-3}
rCS	min.	1.496	29.8×10^{-3}	76.2×10^{-3}	-31.0×10^{-3}
	max.	1.924	81.3×10^{-3}	144.5×10^{-3}	-0.1×10^{-3}
pCS	min.	1.795	0.3×10^{-3}	0.8×10^{-3}	0.1×10^{-3}
	max.	4.460	29.7×10^{-3}	105.6×10^{-3}	3.5×10^{-3}

kcal/mol, resulting in a total energy difference of about 4 kcal/mol (Figures S32 and S33). All in all, despite these differences, the general conclusions of our previous publication do not change. Exergonic reaction pathways remain exergonic and endergonic pathways remain endergonic. The reaction pathway of ORII, which was previously found to be slightly endergonic, is slightly exergonic in our calculations.

QTAIM Atomic Charges and Topological Properties of Bonds Involved in the Reaction Mechanism. Atomic charge variations of atoms and groups of atoms involved in the reaction mechanism are presented in Figure S34. All atomic charges are presented in Table S2. When the TI is formed and a proton is transferred from the hydroxyl group of propranolol to Nπ of H224, there is an electron density transfer from D187 to H224 of about 0.1 au. This is accompanied by an increase of ρ(BCP) of the HB between O of D187 and NτH of H224 by roughly a factor of 2 and a reduction of the HB distance by about 0.2 Å. The change of $H(\mathbf{r}_c)$ shows that this bond becomes more covalent. Within H224, the electron density is transferred to Nπ, increasing its negative charge. On formation of the bond between O2 of propranolol with the electrophilic carbon of acetylated serine, O2 becomes slightly more positively charged by about 0.1 au, maintaining a charge of about −1.0 au. Interestingly, the negative charge in the TI is not localized in the oxygen located in the oxyanion hole but distributed over the whole acetyl group. The additional electron density is mainly received by the carbonyl carbon and the methyl group of the acetyl group. Only very little electron density is received by the carbonyl oxygen located in the oxyanion hole (Figure 4). When the TI is formed, the bond AcS105:C5−AcS105:O5 changes its character from a double to a single bond: its bond distance increases from 1.229 to 1.309 Å, its bond ellipticity decreases from 0.081 to 0.034 au, $\rho(\mathbf{r}_c)$ at this BCP decreases by about 0.05 au, the electron density becomes more localized ($\nabla^2\rho(\mathbf{r}_c)$ becomes more negative), and the electrons are less shared ($H(\mathbf{r}_c)$ increases from −0.74 to −0.58 au).

When the EPC is formed, the following changes can be observed: (i) electron density is transferred from the acetyl group mainly to the oxygen of S105, (changing its charge by about −0.1 au) and to a less extent to the oxygen of propranolol (changing its charge by about −0.06 au). (ii) The bond AcS105:C5−AcS105:O5 changes its character. It becomes shorter by about 0.08 Å, its bond ellipticity increases by 0.05 au, the electron density at the BCP increases by 0.06 au, the electron density becomes less localized ($\nabla^2\rho(\mathbf{r}_c)$ becomes less negative by 0.6 au), and the electrons are more shared ($H(\mathbf{r}_c)$ decreases from −0.58 to −0.75 au). These changes indicate that this bond is a double bond again. (iii) The bonds between AcS105:O4 and AcS105:C5, and between H224:Nπ and H224:NπH are broken, and a proton is transferred from H224 to O4 of S105, recovering the unacetylated serine. (iv) The charge of H224:Nπ becomes more positive again by about 0.08 au. The charge of the rest of the imidazole ring becomes more negative again by about −0.33 au. (v) Negative charge is transferred back to D187 by about −0.03, the HB between D187 and H224 becomes longer by about 0.16 Å, its $\rho(\mathbf{r}_c)$ decreases by about 0.03 au and it becomes less covalent ($H(\mathbf{r}_c)$ decreases from −0.03 to −0.01 au). These changes indicate a weakening of this HB. These results show that D187 acts as an electron density reservoir for H224, and H224 acts as an electron density reservoir for the active site of the protein. It releases electron density when the TI is formed from the MCC and receives it when the EPC is formed.

To get a more coarse grained picture of the charge transfers between propranolol and the active site of CalB, we defined four regions and summed up the atomic charge distribution in each of them. Region I includes propranolol in the MCC and TI. In the TI and EPC, we define a region I′, which consists of acetyl-propranolol. Region II consists of the active site of acetylated CalB in the MCC and TI. Region II′ consists of the active site of CalB in the TI and EPC.

It can be seen that on average an electronic charge of 0.49 au is transferred from the active site of acetylated CalB (region II) to propranolol (region I) when the TI is formed. When the EPC is formed, an electronic charge of about 0.30 is transferred back from acetylated propranolol (region I′) to

https://doi.org/10.1021/acsomega.1c02559
ACS Omega 2021, 6, 20992−21004

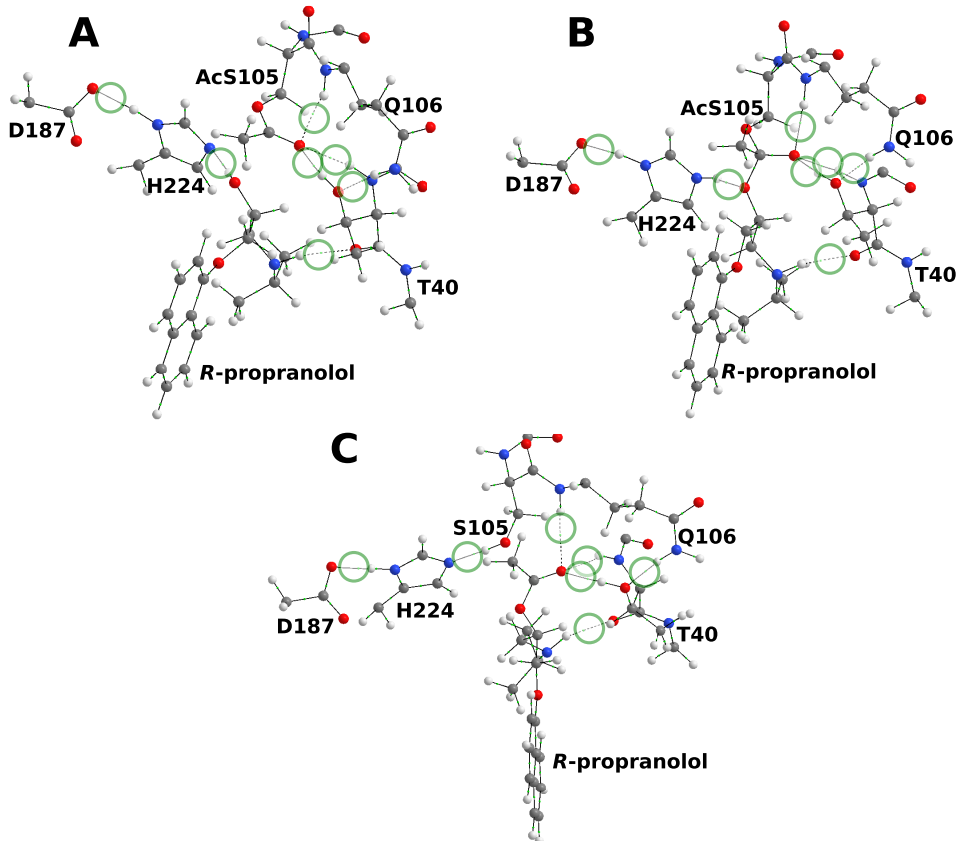

Figure 5. Molecular graphs of the hydrogen bonds studied here, using ORI as an example. Dashed lines correspond to hydrogen bonds. (A) Michaelis complex, (B) tetrahedral intermediate, and (C) enzyme−product complex. Green circles indicate BCPs for hydrogen bonds. White atoms are hydrogen, gray atoms are carbon, red atoms are oxygen, and blue atoms are nitrogen. We note that not in all structures all hydrogen bonds with the oxyanion hole are present (see Table S4).

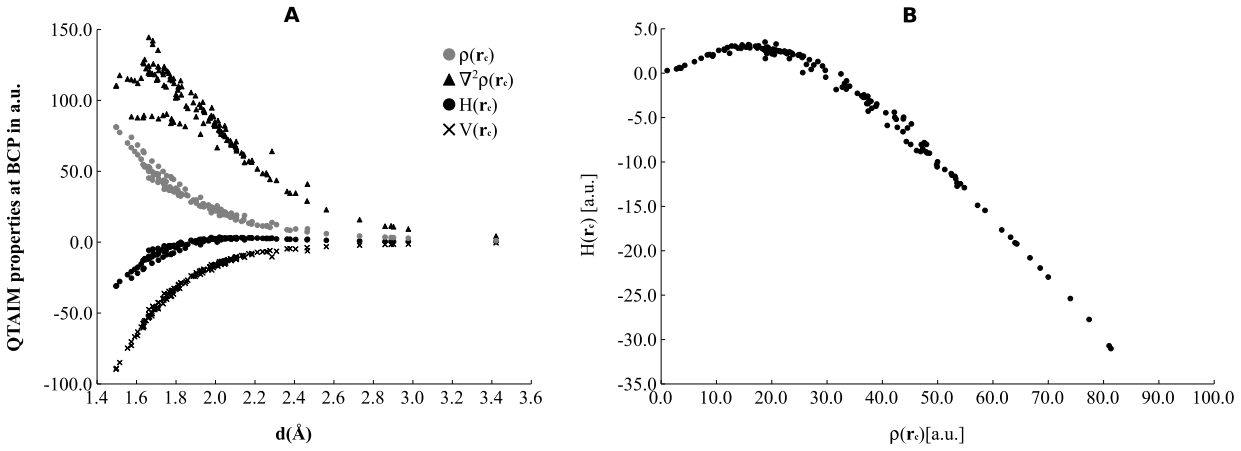

Figure 6. (A) Dependency of QTAIM properties at BCP of all HBs on the hydrogen bond distance (in Å): Laplacian of the electron density (black triangles), electron density (gray circles), total energy density (filled black circles), and potential energy (empty black circles). All QTAIM properties are in au and multiplied by 10^3. (B) Correlation between the electron density and total energy density. All values are given in au × 10^3.

CalB (region II′) (Table S3). We found a weak linear correlation between the amount of charge that is transferred and the QM energy differences (Figures S35 and S36). A more detailed analysis (Table 1) shows that the charge transfer is principally between H224 and propranolol and to a less extent between AcS105/S105 and propranolol/acetylated propranolol (Table 1).

Hydrogen Bonds. We now analyze the interactions in the QM region. In total, 3091 interactions (defined by the existence of a BCP) are found, roughly 130 in the MCC, TI, and EPC of each reaction path. Using Hayashi's scheme,[47] 2624 of these interactions can be classified as shared shell (SS) interactions, 71 as regular closed shell (rCS) interactions, and 396 as pure closed shell (pCS) interactions (Table 2). Shared shell interactions are covalent bonds, with high values of $\rho(\mathbf{r}_c)$, and large and negative $\nabla^2\rho(\mathbf{r}_c)$ and $H(\mathbf{r}_c)$. HBs fall into the last two categories. HBs of the rCS type are also called covalent HBs, while HBs of the pCS type are called ionic HBs. Covalent

https://doi.org/10.1021/acsomega.1c02559
ACS Omega 2021, 6, 20992−21004

Table 3. Representative Geometrical and Topological Properties of the HBs Shown in Figure 5, Using ORI as an Example[a]

path	state	bond	∠(X−H···X)	d (Å)	$\rho(\mathbf{r}_c)$	$\nabla^2\rho(\mathbf{r}_c)$	$H(\mathbf{r}_c)$	HB type
ORI	MCC	Q106:N2H···AcS105:O5	151.1	2.047	21.3	82.1	2.5	pCS
ORI	MCC	T40:N2H···AcS105:O5	162.7	2.132	14.6	63.1	3.2	pCS
ORI	MCC	T40:O1···PRO:NH	167.4	2.106	16.0	66.8	3.1	pCS
ORI	MCC	T40:O3···Q106:N5H	172.9	1.994	22.3	83.5	2.5	pCS
ORI	MCC	D187:O···H224:Nτ*H*	172.2	1.703	48.1	114.4	−9.0	rCS
ORI	MCC	H224:Nπ···PRO:O2H	167.9	1.847	37.4	81.7	−4.3	rCS
ORI	MCC	T40:O3H···AcS105:O5	167.7	1.771	37.6	116.8	−3.1	rCS
ORI	TI	H224:Nπ*H*···PRO:O2	160.1	1.902	27.6	93.6	0.9	pCS
ORI	TI	Q106:N2H···AcS105:O5	170.2	1.964	26.3	85.7	1.0	pCS
ORI	TI	T40:N2H···AcS105:O5	163.6	1.927	25.3	95.2	1.9	pCS
ORI	TI	T40:O1···PRO:NH	165.4	2.075	17.6	71.6	3.1	pCS
ORI	TI	T40:O3···Q106:N5H	172.2	1.998	22.4	82.3	2.4	pCS
ORI	TI	D187:O···H224:Nτ*H*	172.7	1.498	81.0	110.4	−30.7	rCS
ORI	TI	T40:O3H···AcS105:O5	170.2	1.659	51.3	124.0	−10.8	rCS
ORI	EPC	Q106:N2H···PRO:O1c	150.1	2.406	9.3	34.7	1.9	pCS
ORI	EPC	T40:N2H···PRO:O1c	151.8	2.464	7.2	29.1	1.7	pCS
ORI	EPC	T40:O1···PRO:NH	149.8	2.185	14.4	57.7	2.8	pCS
ORI	EPC	T40:O3···Q106:N5H	172.0	1.940	25.0	93.3	2.1	pCS
ORI	EPC	D187:O···H224:Nτ*H*	174.5	1.666	52.6	118.6	−11.5	rCS
ORI	EPC	H224:Nπ···S105:O4H	172.6	1.678	57.2	88.8	−14.9	rCS
ORI	EPC	T40:O3H···PRO:O1c	174.1	1.681	43.8	139.6	−5.1	rCS

[a]The values for all reaction paths are shown in Table S4. All QTAIM properties at the BCP are given in 10^3 au, pCS stands for the pure closed shell, and rCS for regular closed shell.

HBs are characterized by negative $H(\mathbf{r}_c)$ and positive $\nabla^2\rho(\mathbf{r}_c)$. They are also in general shorter than ionic HBs, which are characterized by positive $H(\mathbf{r}_c)$ and positive $\nabla^2\rho(\mathbf{r}_c)$ (see Scheme S1). The HBs that are studied here are the typical HBs like X−H···X (X = O or N) and are of the covalent or ionic type. Figure 5 shows these HBs. More detailed information about the HBs studied herein are shown in Figures S37−S41 and Table S4.

Figure 6A shows the dependency of $\rho(\mathbf{r}_c)$, $\nabla^2\rho(\mathbf{r}_c)$, $H(\mathbf{r}_c)$, and $V(\mathbf{r}_c)$ at the BCP on the bond distance for the hydrogen bonds shown in Figure 5. It can be seen that covalent HBs (characterized by bond distances ≲1.924 Å) are characterized by positive electron densities $\rho(\mathbf{r}_c)$, large positive values of $\nabla^2\rho(\mathbf{r}_c)$, negative $H(\mathbf{r}_c)$ and large negative $V(\mathbf{r}_c)$ at the BCP. At a bond distance >1.924 Å, $H(\mathbf{r}_c)$ becomes positive, which indicates that the electrons at the BCP are not shared (change of the type from rCS to pCS). It can be seen that there is also a correlation between $\rho(\mathbf{r}_c)$ and $H(\mathbf{r}_c)$. This is more evident in Figure 6B, where we plot $H(\mathbf{r}_c)$ against $\rho(\mathbf{r}_c)$. At $\rho(\mathbf{r}_c) = 30 \times 10^{-3}$ au $H(\mathbf{r}_c)$ changes its sign and the type of the HB changes from pCS to rCS. For HBs of type rCS, a nearly linear correlation between $\rho(\mathbf{r}_c)$ and $H(\mathbf{r}_c)$ is observed. At $\rho(\mathbf{r}_c) < 30 \times 10^{-3}$ au, the correlation is parabolic. The maximum of $H(\mathbf{r}_c)$ is observed at 18×10^{-3} au. Topological values such as the HB angle, HB distance, $\rho(\mathbf{r}_c)$, $\nabla^2\rho(\mathbf{r}_c)$ and $H(\mathbf{r}_c)$ of HBs studied herein are presented in Table 3.

In the following, we analyze the HBs of type rCS (covalent HBs) in more detail because these are stabilizing interactions.[85,94] Covalent HBs have been studied computationally and experimentally in various systems,[47,95−101] but to the best of our knowledge, this is the first time that these interactions are studied in the framework of QTAIM in an enzymatic reaction. We start with the hydrogen bonds within the catalytic triad and within the oxyanion hole.

The HB between O of D187 and Nτ*H* of H224 becomes shorter in the TI, where H224 is protonated and longer again in the EPC, where H224 is neutral. These changes are accompanied by variations of $\rho(\mathbf{r}_c)$ by almost a factor of 2, which confirm that this HB is strongest in the TI and second strongest in the EPC. The same tendency is found for $V(\mathbf{r}_c)$. The changes of $\nabla^2\rho(\mathbf{r}_c)$ and $H(\mathbf{r}_c)$ show that the electron density at the BCP is less localized and more shared in the TI than in the MCC and EPC.

The HB between H224 and propranolol is the longest of type rCS (Table 3). In the TI, where the protonated H224 forms a HB with O4 of AcS105 or O2 of propranolol, this HB becomes shorter and is the shortest in the EPC, where S105 forms a HB with H224. This trend of the bond lengths is consistent with the changes of $\rho(\mathbf{r}_c)$, which is the highest in the EPC and the lowest in the MCC. Again, this tendency is also found for $V(\mathbf{r}_c)$. We note that the hydrogen bond between serine and histidine in the EPC is stronger than the hydrogen bond between propranolol and histidine in the MCC, facilitating the release of the acetyl-propranolol. There are no clear trends visible in $\nabla^2\rho(\mathbf{r}_c)$ or in $H(\mathbf{r}_c)$, which indicate that the electron density of these HBs is relatively diffuse and has some covalent character. We also note that in the TI $\rho(\mathbf{r}_c)$ of H224···D187 is higher than that of H224···S105 or H224···PRO in the TI. For the atoms involved in these HBs, we also find the largest variations of atomic charges. It can be seen that the proton transfer from propranolol to H224 is accompanied by a transfer of electron density.

Three HBs may be formed between the carbonyl oxygen and NH or OH of T40 and NH of Q106 in the oxyanion hole. Only one of them (the HB with the OH of T40) is present in the MCC, TI, and EPC of all reaction paths. The other two HBs are present in the MCC and TI of all reaction paths but not in all EPCs. This HB is also the only one that is stabilizing according to the criteria of Cremer and Kraka ($H(\mathbf{r}_c) < 0$).[85] It is the shortest of all three HBs and also has the most negative $V(\mathbf{r}_c)$. In the TI, it is the shortest (average distance 1.656 Å) and the longest in the MCC (average distance 1.784 Å). $\rho(\mathbf{r}_c)$

https://doi.org/10.1021/acsomega.1c02559
ACS Omega 2021, 6, 20992−21004

Table 4. Topological Properties at the BCP of n → π* Interactions[a]

path	state	bond	$\rho(\mathbf{r}_c)$	$\nabla^2\rho(\mathbf{r}_c)$	$V(\mathbf{r}_c)$	$G(\mathbf{r}_c)$	$H(\mathbf{r}_c)$
ORI	MCC	AcS105:C5−PRO:O2	19.9	67.6	−13.1	15.0	1.9
ORII	MCC	AcS105:C5−PRO:O2	13.8	53.1	−9.2	11.2	2.1
ORIII	MCC	AcS105:C5−PRO:O2	13.8	50.9	−8.7	10.7	2.0
ORIV	MCC	AcS105:C5−PRO:O2	9.8	41.6	−6.7	8.5	1.9
OSI	MCC	AcS105:C5−PRO:O2	10.5	39.0	−6.4	8.1	1.7
OSII	MCC	AcS105:C5−PRO:O2	11.3	44.2	−7.3	9.1	1.9
OSIII	MCC	AcS105:C5−PRO:O2					
OSIV	MCC	AcS105:C5−PRO:O2	11.4	43.9	−7.2	9.1	1.9
ORI	EPC	AcPRO:C1−S105:O4	15.1	58.8	−10.2	12.4	2.3
ORIII	EPC	AcPRO:C1−S105:O4	19.1	74.9	−13.9	16.3	2.4
ORIV	EPC	AcPRO:C1−S105:O4					
OSI	EPC	AcPRO:C1−S105:O4	18.5	69.9	−12.9	15.2	2.3
OSII	EPC	AcPRO:C1−S105:O4	11.3	48.7	−8.0	10.1	2.1
OSIII	EPC	AcPRO:C1−S105:O4	13.4	54.6	−9.2	11.4	2.2
OSIV	EPC	AcPRO:C1−S105:O4	17.8	68.1	−12.6	14.8	2.2
ORII	EPC	AcPRO:C1−S105:O4	16.8	66.7	−12.0	14.3	2.3

[a]The units of the QTAIM properties at the BCP are in 10^3 au.

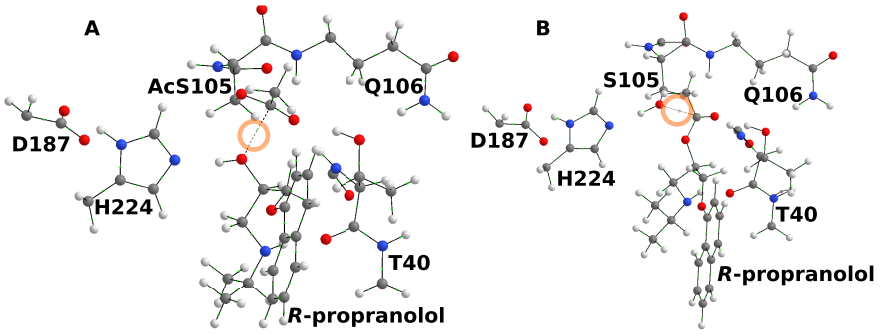

Figure 7. Molecular graph for MCC (A) and EPC (B) of ORI. Dashed lines indicate an n → π* interaction. The orange circles indicate the BCP for the n → π* interaction. White atoms are hydrogen, gray atoms are carbon, red atoms are oxygen, and blue atoms are nitrogen.

of this HB is the largest in the TI and the smallest in the MCC. In addition, we note that in the TI this HB has a lower $\rho(\mathbf{r}_c)$ and less negative $V(\mathbf{r}_c)$ than the HB between D187 and H224, indicating that this H-bond is stronger in the TI than in the MCC and EPC. $\nabla^2\rho(\mathbf{r}_c)$ and $H(\mathbf{r}_c)$ indicate that the electron distribution at the BCP is diffuse and shared, showing some covalency, and that the interaction is stabilizing. The other two HBs are longer, not stabilizing according to the criteria of Cremer and Kraka, and have significantly lower $\rho(\mathbf{r}_c)$ at the BCP. Their $\nabla^2\rho(\mathbf{r}_c)$ indicates that the electron density at the BCP is more diffuse.

There are three HBs that are relevant for the reaction mechanism. These bonds are between D187 and H224 in the TI, H224 and S105 in the EPC, and the carbonyl oxygen and OH of T40 in the oxyanion hole in the TI. The former bond stabilizes the protonated H224 in the TI. The second HB stabilizes the catalytic triad of CalB, facilitating the release of the acylated propranolol. The last bond stabilizes the oxyanion hole in the TI (Figures S37−S41). All three hydrogen bonds are of the covalent type.

Moreover, these results show that the HB between the OH group of T40 and the carbonyl oxygen is the strongest and most important HB in the oxyanion hole. One probable explanation is that the OH group of T40 is in a position that is more favorable for the formation of a HB. Furthermore, because the OH group is part of the side chain, it has more structural flexibility. The NH groups of T40 and Q106 are somewhat more distant, and, being part of the backbone, structurally much less flexible.

From the experimental point of view, the acetylation of (*R*,*S*)-propranolol catalyzed by CalB favors the transformation of (*R*)-propranolol.[102] The enantioselectivity is determined by the changes in the total energy along the reaction path. We did not find correlations between any of the investigated properties and the total energy. We found that the charge transfer between the ligand and the active site correlates with the QM energy. However, as can be seen in Figures S35 and S36, the QM and total energy do not always show the same trend.

n → π* Interactions. We now analyze n → π* interactions, which have been shown to play a role in two scenarios: (i) structure and (ii) reactivity. In the first scenario, this interaction is involved in the stability and preferential conformations of small molecules, peptides,[57,103−106] proteins,[54,106−109] peptoids,[106,110,111] and nucleic acids.[106,112] In the second scenario, the n → π* interactions resemble the Bürgi−Dunitz trajectory for nucleophilic addition to the carbonyl group.[113] In the following, the second scenario will be analyzed. Moreover, the analysis of the n → π* interaction in a biochemical system into the framework of QTAIM is, to our knowledge, the first time.

Table 4 shows selected QTAIM properties at the BCPs between O2 of propranolol and C5 of AcS105 (MCC), and between O4 of S105 and C1b of acetylated propranolol (EPC) for this interaction. It can be seen that $\rho(\mathbf{r}_c)$ at the BCP is not

https://doi.org/10.1021/acsomega.1c02559
ACS Omega 2021, 6, 20992−21004

localized (large values of $\nabla^2\rho(\mathbf{r}_c)$) and is of the pCS type. Furthermore, $\rho(\mathbf{r}_c)$ at the BCP is more diffuse in the interaction between S105 and acetylated propranolol than in the interaction between propranolol and AcS105. Figure 7 shows the n → π^* interactions in the MCC and the EPC.

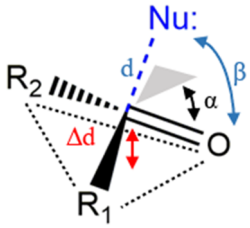

Figure 8. Geometrical parameters that describe a carbonyl group pyramidalization due to an n → π^* interaction.

The geometrical parameters (Figure 8 and Table 5) show that the carbonyl group is slightly nonplanar. The angle α between the plane formed by the substituent atoms of the carbonyl and the carbonyl carbon with the carbonyl group is less than 5.0° and the distance between the central carbon atom and the plane defined by the three atoms bound to it is around 0.12 Å. The range of distances d (2.550−2.955 Å) and the angle β (86.7−98.2°) are consistent with values reported in the literature for this type of interaction.[55,114]

Consistent with the geometrical parameters, the second-order perturbation energies indicate stabilizing n → π^* interactions, with values which have been found for similar systems.[114,115]

CONCLUSIONS

The enzyme−substrate interactions in the enzymatic acylation of (*R*,*S*)-propranolol by CalB were analyzed using QTAIM and NBO. Because these methods are based on quantum mechanics, they give very detailed insight into the interactions and changes of the electronic structure along the reaction path. The starting point of our investigation was the structures obtained in our previous study.[14] To study the electronic structure, it was necessary to extend the QM region, including the residues of the oxyanion hole. The results obtained with the larger QM region are comparable to our previous results.

Our analysis of the electronic structure of the substrate and the active site shows the following:

D187 is an electron density reservoir for H224, and H224 acts as a electron density reservoir for the active site of the protein. It releases electron density when the TI is formed and recovers it when the EPC is formed.

All hydrogen bonds within the catalytic triad and between the enzyme and propranolol are covalent or ionic hydrogen bonds. The covalent hydrogen bonds are characterized by bond distances between 1.496 and 1.924 Å, $\rho(\mathbf{r}_c)$ between 29.8 × 10^{-3} and 81.3 × 10^{-3} au, $\nabla^2\rho(\mathbf{r}_c)$ between 76.2 × 10^{-3} and 144.5 × 10^{-3} au, and $H(\mathbf{r}_c)$ between −31.0 × 10^{-3} and −0.1 × 10^{-3} au. This indicates depleted $\rho(\mathbf{r}_c)$, shared shell interactions, some bond covalency, and stabilizing features. These are the strongest HBs because they have a higher electron density and shorter bond length than the ionic hydrogen bonds. Such HBs are found between D187 and H224, between PRO and H224, T40:OH and AcS105, and between H224 and S105. Ionic hydrogen bonds (characterized by distances between 1.795 and 4.460 Å, $\rho(\mathbf{r}_c)$ between 0.3 × 10^{-3} and 29.7 × 10^{-3} au, $\nabla^2\rho(\mathbf{r}_c)$ between 0.8 × 10^{-3} and 105.6 × 10^{-3} au, and $H(\mathbf{r}_c)$ between 0.1 × 10^{-3} and 3.5 × 10^{-3} au) are weaker than covalent hydrogen bonds. These hydrogen bonds are formed, for example, between T40:NH or Q106:NH and AcS105 or PRO.

n → π^* interactions between the OH oxygen of propranolol and the carbonyl group of the acyl serine in the MCC, and between the OH oxygen of serine and the carbonyl group of the acylated propranolol in the EPC were found and characterized by their geometric and QTAIM and NBO parameters. The geometrical and NBO parameters are in the range of typical n → π^* interactions. In the QTAIM framework, these interactions are of the pCS type, with $\rho(\mathbf{r}_c)$ between 9.8 × 10^{-3} and 19.9 × 10^{-3} au, $\nabla^2\rho(\mathbf{r}_c)$ between 39.0 × 10^{-3} and 74.9 × 10^{-3} au, and $H(\mathbf{r}_c)$ between 1.7 × 10^{-3} and 2.4 × 10^{-3} au. The Bürgi−Dunitz bond distances are between 2.550 and 2.955 Å. The electron density of these interactions is more diffuse in the interactions between serine and acylated

Table 5. Values of the Geometrical Parameters Shown in Figure 8 for Each n → π^* Interaction in the MCC and EPC[a]

path	state	bond	d (Å)	Δd (Å)	α (deg)	β (deg)	ΔE (kcal/mol)	ΔE (kcal/mol)	$\sum(\Delta E)$ (kcal/mol)
ORI	MCC	AcS105:C5−PRO:O2	2.550	0.13	5.0	98.0	0.66	1.87	2.53
ORII	MCC	AcS105:C5−PRO:O2	2.699	0.12	1.5	93.9	0.61	0.43	1.04
ORIII	MCC	AcS105:C5−PRO:O2	2.701	0.15	4.6	92.2	0.56	0.66	1.22
ORIV	MCC	AcS105:C5−PRO:O2	2.955	0.13	2.7	96.5	0.30		0.30
OSI	MCC	AcS105:C5−PRO:O2	2.863	0.13	2.1	92.4	0.22	0.32	0.54
OSII	MCC	AcS105:C5−PRO:O2	2.805	0.12	3.5	98.2	0.57		0.57
OSIII	MCC	AcS105:C5−PRO:O2		0.12	0.2				
OSIV	MCC	AcS105:C5−PRO:O2	2.775	0.11	1.7	92.3	0.49	0.25	0.74
ORI	EPC	AcPRO:C1−S105:O4	2.650	0.14	2.5	90.8	0.97	0.07	1.04
ORII	EPC	AcPRO:C1−S105:O4	2.581	0.13	2.1	95.1	1.17	0.36	1.53
ORIII	EPC	AcPRO:C1−S105:O4	2.567	0.08	3.2	86.2	1.01	0.56	1.57
ORIV	EPC	AcPRO:C1−S105:O4		0.13	1.2				
OSI	EPC	AcPRO:C1−S105:O4	2.585	0.08	3.1	88.1	0.78	0.85	1.63
OSII	EPC	AcPRO:C1−S105:O4	2.876	0.13	1.4	86.7	0.33		0.33
OSIII	EPC	AcPRO:C1−S105:O4	2.685	0.14	1.9	93.9	0.82		0.82
OSIV	EPC	AcPRO:C1−S105:O4	2.577	0.13	1.9	95.0	0.88	0.33	1.21

[a]NBO second-order perturbation energies ΔE of the occupied oxygen n orbitals with an unoccupied carbonyl π^* orbital are also shown.

https://doi.org/10.1021/acsomega.1c02559
ACS Omega 2021, 6, 20992−21004

propranolol than in the interaction between propranolol and acyl serine.

■ ASSOCIATED CONTENT

Supporting Information

The Supporting Information is available free of charge at https://pubs.acs.org/doi/10.1021/acsomega.1c02559.

$H(\mathbf{r}_c)$ and $H(\mathbf{r}_c) - V(\mathbf{r}_c)/2$ values define four quadrants (Scheme S1); atom numbering of aspartic acid, serine, acetyl-serine, glutamine, histidine, (*R*,*S*)-propranolol, and (*R*,*S*)-acetyl-propranolol (Figures S1−S7); QM-(B3LYP/TZVP)/MM energy profiles for the conversion of (*R*)- (left) and (*S*)-propranolol (right) to *O*-acetyl-propranolol in binding modes I and II (Figure S8); superposition of the structures obtained in the previous study[2] and the present study for the MCC, TI, and EPC of ORI−ORIV and OSI-OSIV (Figures S9−S32); RMSD (in Å, with respect to the geometries obtained in the previous study[2]) of the residues within 7 Å of the substrate at the stationary points along the reaction profiles of ORI-IV and OSI-IV: MCC (blue), TI (orange) and EPC (gray) (Figure S33); sum of atomic charges for fragments and individual atoms (Figure S34); correlation between the relative QM energy ΔE (with respect to the MCC) and the difference of the sum of atomic charges for regions II and II′ (Figures S35 and S37); QTAIM topological properties for the hydrogen bond formed (Figures S37−S41); QM(B3LYP/TZVP) and MM(CHARMM) energies in kcal/mol (relative to the MCC) for the transformation of (*R*,*S*)-propranolol in binding modes I and II (Table S1); atomic charges for all atoms in the MCC, TI and EPC for each reaction path (Table S2); sum of atomic charges for the defined regions in the QM region (Table S3); geometrical parameters, QTAIM properties at the BCP (in au × 10^3) and classification of selected hydrogen bonds (Table S4); and QTAIM properties at the BCP (in au × 10^3) and binding energy (in kcal/mol), calculated from $V(\mathbf{r}_c)$ (Table S5) (PDF)

All optimized structures in PDB format (ZIP)

■ AUTHOR INFORMATION

Corresponding Author

Markus Doerr − *Grupo de Bioquímica Teórica, Universidad Industrial de Santander, Bucaramanga 680002, Colombia;* orcid.org/0000-0003-1001-2972; Phone: 57 7 6344000; Email: mhodoerr@uis.edu.co

Authors

David A. Rincón − *Grupo de Bioquímica Teórica, Universidad Industrial de Santander, Bucaramanga 680002, Colombia;* orcid.org/0000-0002-0429-9420

Martha C. Daza − *Grupo de Bioquímica Teórica, Universidad Industrial de Santander, Bucaramanga 680002, Colombia;* orcid.org/0000-0001-6464-7469

Complete contact information is available at: https://pubs.acs.org/10.1021/acsomega.1c02559

Notes

The authors declare no competing financial interest.

■ ACKNOWLEDGMENTS

D.A.R. acknowledges financial support from MINCIENCIAS: Fondo Nacional de Financiamiento para la Ciencia, la Tecnología y la Innovación "Francisco José de Caldas" (Convocatoria 848 del 2019 Programa de Estancias Post-doctorales) and from Universidad Industrial de Santander, projects VIE-UIS 007-2020/2020000274 and VIE-UIS 002-2021-CPP/2021000079. Financial support from MINCIENCIAS, grant number 110271250586 and from Universidad Industrial de Santander (VIE-UIS 8855) is also acknowledged.

■ REFERENCES

(1) Erhardt, P. W.; Woo, C. M.; Gorczynski, R. J.; Anderson, W. G. Ultra-Short-Acting.Beta.-Adrenergic Receptor Blocking Agents. 1. (Aryloxy)Propanolamines Containing Esters in the Nitrogen Substituent. *J. Med. Chem.* **1982**, *25*, 1402−1407.

(2) Kopka, K.; Wagner, S.; Riemann, B.; Law, M. P.; Puke, C.; Luthra, S. K.; Pike, V. W.; Wichter, T.; Schmitz, W.; Schober, O.; Schäfers, M. Design of New B1-Selective Adrenoceptor Ligands as Potential Radioligands for in Vivo Imaging. *Bioorg. Med. Chem.* **2003**, *11*, 3513−3527.

(3) Slater, R. A.; Howson, W.; Swayne, G. T. G.; Taylor, E. M.; Reavill, D. R. Design and Synthesis of a Series of Combined Vasodilator-.Beta.-Adrenoceptor Antagonists Based on 6-Arylpyridazinones. *J. Med. Chem.* **1988**, *31*, 345−351.

(4) Borude, V. S.; Shah, R. V.; Shukla, S. R. Synthesis of B-Amino Alcohol Derivatives from Phenols in Presence of Phase Transfer Catalyst and Lipase Biocatalyst. *Curr. Chem. Lett.* **2013**, *2*, 1−12.

(5) Gallego, J. M. L.; Pérez Arroyo, J. Determination of Prednisolone, Naphazoline, and Phenylephrine in Local Pharmaceutical Preparations by Micellar Electrokinetic Chromatography. *J. Sep. Sci.* **2003**, *26*, 947−952.

(6) Klingler, F. D. Asymmetric Hydrogenation of Prochiral Amino Ketones to Amino Alcohols for Pharmaceutical Use. *Acc. Chem. Res.* **2007**, *40*, 1367−1376.

(7) Castellano, M.; Böhm, M. The Cardiac Beta-Adrenoceptor-Mediated Signaling Pathway and Its Alterations in Hypertensive Heart Disease. *Hypertension* **1997**, *29*, 715−722.

(8) Yamada, S.; Ohkura, T.; Uchida, S.; Inabe, K.; Iwatani, Y.; Kimura, R.; Hoshino, T.; Kaburagi, T. A Sustained Increase in *β*-Adrenoceptors during Long-Term Therapy with Metoprolol and Bisoprolol in Patients with Heart Failure from Idiopathic Dilated Cardiomyopathy. *Life Sci.* **1996**, *58*, 1737−1744.

(9) Auvin-Guette, C.; Rebuffat, S.; Prigent, Y.; Bodo, B. Trichogin A IV, an 11-Residue Lipopeptaibol from *Trichoderma longibrachiatum*. *J. Am. Chem. Soc.* **1992**, *114*, 2170−2174.

(10) Turner, P.; Granville-Grossman, K. L.; Smart, J. V. Effect of Adrenergic Receptor Blockade on the Tachycardia of Thyrotoxicosis and Anxiety State. *Lancet* **1965**, *286*, 1316−1318.

(11) Barrett, A. M. Cardiac Beta-Adrenoceptor Blockade: The Quest for Selectivity. *J. Pharmacol.* **1985**, *16*, 95−108.

(12) Rabkin, R.; Stables, D. P.; Levin, N. W.; Suzman, M. M. The Prophylactic Value of Propranolol in Angina Pectoris. *Am. J. Cardiol.* **1966**, *18*, 370−380.

(13) Besterman, E. M.; Friedlander, D. H. Clinical Experiences with Propranolol. *Postgrad. Med. J.* **1965**, *41*, 526.

(14) Escorcia, A. M.; Sen, K.; Daza, M. C.; Doerr, M.; Thiel, W. Quantum Mechanics/Molecular Mechanics Insights into the Enantioselectivity of the O-Acetylation of (R,S)-Propranolol Catalyzed by *Candida antarctica* Lipase B. *ACS Catal.* **2017**, *7*, 115−127.

(15) Ram, C. V. S. Risk of New-Onset Diabetes Mellitus in Patients With Hypertension Treated With Beta Blockers. *Am. J. Cardiol.* **2008**, *102*, 242−244.

(16) Belknap, S. Review: Beta-Blockers for Hypertension Increase Risk of New Onset Diabetes. *Evidence-Based Med.* **2008**, *13*, 50.

(17) Patakas, D.; Argiropoulou, V.; Louridas, G.; Tsara, V. Beta-Blockers in Bronchial Asthma: Effect of Propranolol and Pindolol on Large and Small Airways. *Thorax* **1983**, *38*, 108−112.
(18) Absalan, G.; Akhond, M.; Rafatmah, E.; Alipour, Y. Application of Gold Nanoparticles and L-Cysteine Double Layer on Commercial Thin-Layer Chromatography Plates as a New Substrate for Direct Resolution of Propranolol Enantiomers. *J. Planar Chromatogr.—Mod. TLC* **2014**, *27*, 409−415.
(19) Bhushan, R.; Tanwar, S. Direct TLC Resolution of Atenolol and Propranolol into Their Enantiomers Using Three Different Chiral Selectors as Impregnating Reagents. *Biomed. Chromatogr.* **2008**, *22*, 1028−1034.
(20) Bhushan, R.; Arora, M. Direct Enantiomeric Resolution of (+/-)-Atenolol, (+/-)-Metoprolol, and (+/-)-Propranolol by Impregnated TLC Using L-Aspartic Acid as Chiral Selector. *Biomed. Chromatogr.* **2003**, *17*, 226−230.
(21) Yadav, J. S.; Reddy, A. R.; Narsaiah, A. V.; Reddy, B. V. S. An Efficient Protocol for Regioselective Ring Opening of Epoxides Using Samarium Triflate: Synthesis of Propranolol, Atenolol and RO363. *J. Mol. Catal. A: Chem.* **2007**, *261*, 207−212.
(22) Pathare, S. P.; Akamanchi, K. G. An Efficient Protocol for Regioselective Ring Opening of Epoxides Using Sulfated Tungstate: Application in Synthesis of Active Pharmaceutical Ingredients Atenolol, Propranolol and Ranolazine. *Tetrahedron Lett.* **2013**, *54*, 6455−6459.
(23) Lagos, F. M.; Carballeira, J. D.; Bermudez, J. L.; Alvarez, E.; Sinisterra, J. V. Highly Stereoselective Reduction of Haloketones Using Three New Yeasts: Application to the Synthesis of (S)-Adrenergic Beta-Blockers Related to Propranolol. *Tetrahedron: Asymmetry* **2004**, *15*, 763−770.
(24) Panchgalle, S. P.; Gore, R. G.; Chavan, S. P.; Kalkote, U. R. Organocatalytic Enantioselective Synthesis of Beta-Blockers: (S)-Propranolol and (S)-Naftopidil. *Tetrahedron: Asymmetry* **2009**, *20*, 1767−1770.
(25) Barbosa, O.; Ariza, C.; Ortiz, C.; Torres, R. Kinetic Resolution of (R/S)-Propranolol (1-Isopropylamino-3-(1-Naphtoxy)-2-Propanolol) Catalyzed by Immobilized Preparations of *Candida antarctica* Lipase B (CAL-B). *New Biotechnol.* **2010**, *27*, 844−850.
(26) Barbosa, O.; Torres, R.; Ortiz, C. Kinetic Resolution of (R/S)-Propranolol by Immobilized Preparations of Lipase from *Candida antarctica* B. *New Biotechnol.* **2009**, *25*, S113.
(27) Kamal, A.; Sandbhor, M.; Shaik, A. Chemoenzymatic Synthesis of (S) and (R)-Propranolol and Sotalol Employing One-Pot Lipase Resolution Protocol. *Bioorg. Med. Chem. Lett.* **2004**, *14*, 4581−4583.
(28) Hüttner, S.; Gomes, M. Z. D. V.; Iancu, L.; Palmqvist, A.; Olsson, L. Immobilisation on Mesoporous Silica and Solvent Rinsing Improve the Transesterification Abilities of Feruloyl Esterases from Myceliophthora Thermophila. *Bioresour. Technol.* **2017**, *239*, 57−65.
(29) Thörn, C.; Gustafsson, H.; Olsson, L. Immobilization of Feruloyl Esterases in Mesoporous Materials Leads to Improved Transesterification Yield. *J. Mol. Catal. B: Enzym.* **2011**, *72*, 57−64.
(30) Topakas, E.; Stamatis, H.; Biely, P.; Kekos, D.; Macris, B. J.; Christakopoulos, P. Purification and Characterization of a Feruloyl Esterase from Fusarium Oxysporum Catalyzing Esterification of Phenolic Acids in Ternary Water-Organic Solvent Mixtures. *J. Biotechnol.* **2003**, *102*, 33−44.
(31) Topakas, E.; Stamatis, H.; Mastihubova, M.; Biely, P.; Kekos, D.; Macris, B. J.; Christakopoulos, P. Purification and Characterization of a Fusarium Oxysporum Feruloyl Esterase (FoFAE-I) Catalysing Transesterification of Phenolic Acid Esters. *Enzyme Microb. Technol.* **2003**, *33*, 729−737.
(32) Tsuchiyama, M.; Sakamoto, T.; Fujita, T.; Murata, S.; Kawasaki, H. Esterification of Ferulic Acid with Polyols Using a Ferulic Acid Esterase from Aspergillus Niger. *Biochim. Biophys. Acta, Gen. Subj.* **2006**, *1760*, 1071−1079.
(33) Holland, R.; Liu, S. Q.; Crow, V. L.; Delabre, M. L.; Lubbers, M.; Bennett, M.; Norris, G. Esterases of Lactic Acid Bacteria and Cheese Flavour: Milk Fat Hydrolysis, Alcoholysis and Esterification. *Int. Dairy J.* **2005**, *15*, 711−718.
(34) Ribitsch, D.; Herrero Acero, E.; Greimel, K.; Dellacher, A.; Zitzenbacher, S.; Marold, A.; Rodriguez, R. D.; Steinkellner, G.; Gruber, K.; Schwab, H.; Guebitz, G. M. A New Esterase from Thermobifida Halotolerans Hydrolyses Polyethylene Terephthalate (PET) and Polylactic Acid (PLA). *Polymers* **2012**, *4*, 617−629.
(35) Vega, D.; Bastide, J. Dimethylphthalate Hydrolysis by Specific Microbial Esterase. *Chemosphere* **2003**, *51*, 663−668.
(36) van Tienhoven, M.; Atkins, J.; Li, Y.; Glynn, P. Human Neuropathy Target Esterase Catalyzes Hydrolysis of Membrane Lipids. *J. Biol. Chem.* **2002**, *277*, 20942−20948.
(37) Ghanem, A. Trends in Lipase-Catalyzed Asymmetric Access to Enantiomerically Pure/Enriched Compounds. *Tetrahedron* **2007**, *63*, 1721−1754.
(38) Ravot, G.; Buteux, D.; Favre-Bulle, O.; Wahler, D.; Veit, T.; Lefèvre, F. Screening for Thermostable Esterases: From Deep Sea to Industry. *Eng. Life Sci.* **2004**, *4*, 533−538.
(39) Ishii, M. Positionally Non-Specific Lipase from Candida Sp, a Method for Producing It, Its Use and a Recombinant DNA Process for Producing It. WO1988002775, 1987.
(40) Hedstrom, L. Serine Protease Mechanism and Specificity. *Chem. Rev.* **2002**, *102*, 4501−4523.
(41) Escorcia, A. M.; Molina, D.; Daza, M. C.; Doerr, M. Acetylation of (R,S)-Propranolol Catalyzed by *Candida antarctica* Lipase B: An Experimental and Computational Study. *J. Mol. Catal. B: Enzym.* **2013**, *98*, 21−29.
(42) Escorcia, A. M.; Daza, M. C.; Doerr, M. Computational Study of the Enantioselectivity of the O-Acetylation of (R,S)-Propranolol Catalyzed by *Candida antarctica* Lipase B. *J. Mol. Catal. B: Enzym.* **2014**, *108*, 21−31.
(43) Bader, R. F. W. *Atoms in Molecules: A Quantum Theory*; International Series of Monographs on Chemistry; Clarendon Press, 1994.
(44) Bader, R. F. W. A Quantum Theory of Molecular Structure and Its Applications. *Chem. Rev.* **1991**, *91*, 893−928.
(45) Khrenova, M. G.; Krivitskaya, A. V.; Tsirelson, V. G. The QM/MM-QTAIM Approach Reveals the Nature of the Different Reactivity of Cephalosporins in the Active Site of L1 Metallo-β-Lactamase. *New J. Chem.* **2019**, *43*, 7329−7338.
(46) Espinosa, E.; Alkorta, I.; Elguero, J.; Molins, E. From Weak to Strong Interactions: A Comprehensive Analysis of the Topological and Energetic Properties of the Electron Density Distribution Involving X−H···F−Y Systems. *J. Chem. Phys.* **2002**, *117*, 5529−5542.
(47) Hayashi, S.; Matsuiwa, K.; Kitamoto, M.; Nakanishi, W. Dynamic Behavior of Hydrogen Bonds from Pure Closed Shell to Shared Shell Interaction Regions Elucidated by AIM Dual Functional Analysis. *J. Phys. Chem. A* **2013**, *117*, 1804−1816.
(48) Rodriguez-Serrano, A.; Daza, M. C.; Doerr, M.; Villaveces, J. L. Proton transfer from 1,4-pentadiene to superoxide radical anion: a QTAIM analysis. *Rev. Colomb. Quim.* **2012**, *41*, 409−432.
(49) Königstein, M.; Sokol, A. A.; Catlow, C. R. A. Electronic Structure and Bonding in Crystalline Peroxides. *Phys. Rev. B* **1999**, *60*, 4594−4604.
(50) Luchi, A. M.; Angelina, E. L.; Andujar, S. A.; Enriz, R. D.; Peruchena, N. M. Halogen Bonding in Biological Context: A Computational Study of D2 Dopamine Receptor. *J. Phys. Org. Chem.* **2016**, *29*, 645−655.
(51) Campos, L. E.; Garibotto, F. M.; Angelina, E.; Kos, J.; Tomašič, T.; Zidar, N.; Kikelj, D.; Gonec, T.; Marvanova, P.; Mokry, P.; Jampilek, J.; Alvarez, S. E.; Enriz, R. D. Searching New Structural Scaffolds for BRAF Inhibitors. An Integrative Study Using Theoretical and Experimental Techniques. *Bioorg. Chem.* **2019**, *91*, No. 103125.
(52) Malek Zadeh, S.; Astani, E. K.; Wang, Z.-C.; Adhikari, K.; Rattinam, R.; Li, T.-L. Theoretical Study of Intermolecular Interactions between Critical Residues of Membrane Protein MraYAA and Promising Antibiotic Muraymycin D2. *ACS Omega* **2020**, *5*, 22739−22749.
(53) Rojas, S.; Parravicini, O.; Vettorazzi, M.; Tosso, R.; Garro, A.; Gutiérrez, L.; Andújar, S.; Enriz, R. Combined MD/QTAIM

https://doi.org/10.1021/acsomega.1c02559
ACS Omega 2021, 6, 20992−21004

Techniques to Evaluate Ligand-Receptor Interactions. Scope and Limitations. *Eur. J. Med. Chem.* **2020**, *208*, No. 112792.
(54) Bartlett, G. J.; Choudhary, A.; Raines, R. T.; Woolfson, D. N. N→π* Interactions in Proteins. *Nat. Chem. Biol.* **2010**, *6*, 615−620.
(55) Choudhary, A.; Newberry, R. W.; Raines, R. T. N→π* Interactions Engender Chirality in Carbonyl Groups. *Org. Lett.* **2014**, *16*, 3421−3423.
(56) Newberry, R. W.; Raines, R. T. The N→π* Interaction. *Acc. Chem. Res.* **2017**, *50*, 1838−1846.
(57) Sahariah, B.; Sarma, B. K. Spectroscopic Evidence of n → Π* Interactions Involving Carbonyl Groups. *Phys. Chem. Chem. Phys.* **2020**, *22*, 26669−26681.
(58) Uppenberg, J.; Hansen, M. T.; Patkar, S.; Jones, T. A. The Sequence, Crystal Structure Determination and Refinement of Two Crystal Forms of Lipase B from *Candida antarctica*. *Structure* **1994**, *2*, 293−308.
(59) Jurrus, E.; Engel, D.; Star, K.; Monson, K.; Brandi, J.; Felberg, L. E.; Brookes, D. H.; Wilson, L.; Chen, J.; Liles, K.; Chun, M.; Li, P.; Gohara, D. W.; Dolinsky, T.; Konecny, R.; Koes, D. R.; Nielsen, J. E.; Head-Gordon, T.; Geng, W.; Krasny, R.; Wei, G.; Holst, M. J.; McCammon, J. A.; Baker, N. A. Improvements to the APBS Biomolecular Solvation Software Suite. *Protein Sci.* **2018**, *27*, 112−128.
(60) Dolinsky, T. J.; Czodrowski, P.; Li, H.; Nielsen, J. E.; Jensen, J. H.; Klebe, G.; Baker, N. A. PDB2PQR: Expanding and Upgrading Automated Preparation of Biomolecular Structures for Molecular Simulations. *Nucleic Acids Res.* **2007**, *35*, W522−W525.
(61) Dolinsky, T. J.; Nielsen, J. E.; McCammon, J. A.; Baker, N. A. PDB2PQR: An Automated Pipeline for the Setup of Poisson-Boltzmann Electrostatics Calculations. *Nucleic Acids Res.* **2004**, *32*, W665−W667.
(62) Li, H.; Robertson, A. D.; Jensen, J. H. Very Fast Empirical Prediction and Rationalization of Protein PKa Values. *Proteins: Struct., Funct., Bioinf.* **2005**, *61*, 704−721.
(63) Bas, D. C.; Rogers, D. M.; Jensen, J. H. Very Fast Prediction and Rationalization of PKa Values for Protein-Ligand Complexes. *Proteins: Struct., Funct., Bioinf.* **2008**, *73*, 765−783.
(64) Davis, A. M.; Teague, S. J. Hydrogen Bonding, Hydrophobic Interactions, and Failure of the Rigid Receptor Hypothesis. *Angew. Chem., Int. Ed.* **1999**, *38*, 736−749.
(65) Becke, A. D. Density-functional Thermochemistry. III. The Role of Exact Exchange. *J. Chem. Phys.* **1993**, *98*, 5648−5652.
(66) Lee, C.; Yang, W.; Parr, R. G. Development of the Colle-Salvetti Correlation-Energy Formula into a Functional of the Electron Density. *Phys. Rev. B* **1988**, *37*, 785−789.
(67) Vosko, S. H.; Wilk, L.; Nusair, M. Accurate Spin-Dependent Electron Liquid Correlation Energies for Local Spin Density Calculations: A Critical Analysis. *Can. J. Phys.* **1980**, *58*, 1200−1211.
(68) Stephens, P. J.; Devlin, F. J.; Chabalowski, C. F.; Frisch, M. J. Ab Initio Calculation of Vibrational Absorption and Circular Dichroism Spectra Using Density Functional Force Fields. *J. Phys. Chem. A* **1994**, *98*, 11623−11627.
(69) Schäfer, A.; Huber, C.; Ahlrichs, R. Fully Optimized Contracted Gaussian Basis Sets of Triple Zeta Valence Quality for Atoms Li to Kr. *J. Chem. Phys.* **1994**, *100*, 5829−5835.
(70) Neese, F. The ORCA Program System. *WIREs Comput. Mol. Sci.* **2012**, *2*, 73−78.
(71) Neese, F. Software Update: The ORCA Program System, Version 4.0. *WIREs Comput. Mol. Sci.* **2018**, *8*, No. e1327.
(72) Neese, F.; Wennmohs, F.; Becker, U.; Riplinger, C. The ORCA Quantum Chemistry Program Package. *J. Chem. Phys.* **2020**, *152*, No. 224108.
(73) Bakowies, D.; Thiel, W. Hybrid Models for Combined Quantum Mechanical and Molecular Mechanical Approaches. *J. Phys. Chem. A* **1996**, *100*, 10580−10594.
(74) de Vries, A. H.; Sherwood, P.; Collins, S. J.; Rigby, A. M.; Rigutto, M.; Kramer, G. J. Zeolite Structure and Reactivity by Combined Quantum-Chemical−Classical Calculations. *J. Phys. Chem. B* **1999**, *103*, 6133−6141.
(75) Sherwood, P.; de Vries, A. H.; J Collins, S.; P Greatbanks, S.; A Burton, N.; A Vincent, M.; H Hillier, I. Computer Simulation of Zeolite Structure and Reactivity Using Embedded Cluster Methods. *Faraday Discuss.* **1997**, *106*, 79−92.
(76) Huang, J.; MacKerell, A. D., Jr. CHARMM36 All-Atom Additive Protein Force Field: Validation Based on Comparison to NMR Data. *J. Comput. Chem.* **2013**, *34*, 2135−2145.
(77) Grimme, S.; Bannwarth, C.; Shushkov, P. A Robust and Accurate Tight-Binding Quantum Chemical Method for Structures, Vibrational Frequencies, and Noncovalent Interactions of Large Molecular Systems Parametrized for All Spd-Block Elements (Z = 1−86). *J. Chem. Theory Comput.* **2017**, *13*, 1989−2009.
(78) Bannwarth, C.; Ehlert, S.; Grimme, S. GFN2-XTB—An Accurate and Broadly Parametrized Self-Consistent Tight-Binding Quantum Chemical Method with Multipole Electrostatics and Density-Dependent Dispersion Contributions. *J. Chem. Theory Comput.* **2019**, *15*, 1652−1671.
(79) Caldeweyher, E.; Ehlert, S.; Hansen, A.; Neugebauer, H.; Spicher, S.; Bannwarth, C.; Grimme, S. A Generally Applicable Atomic-Charge Dependent London Dispersion Correction. *J. Chem. Phys.* **2019**, *150*, No. 154122.
(80) Grimme, S.; Bannwarth, C. Ultra-Fast Computation of Electronic Spectra for Large Systems by Tight-Binding Based Simplified Tamm-Dancoff Approximation (STDA-XTB). *J. Chem. Phys.* **2016**, *145*, No. 054103.
(81) Spicher, S.; Grimme, S. Robust Atomistic Modeling of Materials, Organometallic, and Biochemical Systems. *Angew. Chem., Int. Ed.* **2020**, *59*, 15665−15673.
(82) Bannwarth, C.; Caldeweyher, E.; Ehlert, S.; Hansen, A.; Pracht, P.; Seibert, J.; Spicher, S.; Grimme, S. Extended tight-binding Quantum Chemistry Methods. *WIREs Comput. Mol. Sci.* **2021**, *11*, No. e1493.
(83) Brandenburg, J. G.; Bannwarth, C.; Hansen, A.; Grimme, S. B97-3c: A Revised Low-Cost Variant of the B97-D Density Functional Method. *J. Chem. Phys.* **2018**, *148*, No. 064104.
(84) Keith, T. A. *AIMAll*; TK Gristmill Software: Overland Park, KS, 2013.
(85) Cremer, D.; Kraka, E. A Description of the Chemical Bond in Terms of Local Properties of Electron Density and Energy. *Croat. Chem. Acta* **1984**, *57*, 1259−1281.
(86) Glendening, E. D.; Badenhoop, J. K.; Reed, A. E.; Carpenter, J. E.; Bohmann, J. A.; Morales, C. M.; Karafiloglou, P.; Landis, C. R.; Weinhold, F. *NBO*, version 7.0; Theoretical Chemistry Institute, University of Wisconsin: Madison, 2018.
(87) Humphrey, W.; Dalke, A.; Schulten, K. VMD: Visual Molecular Dynamics. *J. Mol. Graphics* **1996**, *14*, 33−38.
(88) Kim, Y.; Ahn, K.-H. Theoretical Study of the Role of Low-Barrier Hydrogen Bonds in Enzyme Catalysis: A Model of Proton Transfer in Serine Protease. *Theor. Chem. Acc.* **2001**, *106*, 171−177.
(89) Cleland, W. W.; Frey, P. A.; Gerlt, J. A. The Low Barrier Hydrogen Bond in Enzymatic Catalysis. *J. Biol. Chem.* **1998**, *273*, 25529−25532.
(90) Wilmouth, R. C.; Edman, K.; Neutze, R.; Wright, P. A.; Clifton, I. J.; Schneider, T. R.; Schofield, C. J.; Hajdu, J. X-Ray Snapshots of Serine Protease Catalysis Reveal a Tetrahedral Intermediate. *Nat. Struct. Biol.* **2001**, *8*, 689−694.
(91) Kumar, P.; Agarwal, P. K.; Cuneo, M. J. On the Case of the Misplaced Hydrogens. *ChemBioChem* **2021**, *22*, 288−297.
(92) Everill, P.; Sudmeier, J. L.; Bachovchin, W. W. Direct NMR Observation and pK_a Determination of the Asp^{102} Side Chain in a Serine Protease. *J. Am. Chem. Soc.* **2012**, *134*, 2348−2354.
(93) Agback, P.; Agback, T. Direct Evidence of a Low Barrier Hydrogen Bond in the Catalytic Triad of a Serine Protease. *Sci. Rep.* **2018**, *8*, No. 10078.
(94) Gibbs, G. V.; et al. Bonded Interactions and the Crystal Chemistry of Minerals: A Review. *Z. Kristallogr. − Cryst. Mater.* **2008**, *223*, 1−40.
(95) Gilli, G.; Gilli, P. Towards an Unified Hydrogen-Bond Theory. *J. Mol. Struct.* **2000**, *552*, 1−15.

https://doi.org/10.1021/acsomega.1c02559
ACS Omega 2021, 6, 20992−21004

(96) Onoda, A.; Yamada, Y.; Takeda, J.; Nakayama, Y.; Okamura, T.; Doi, M.; Yamamoto, H.; Ueyama, N. Stabilization of Carboxylate Anion with a NH···O Hydrogen Bond: Facilitation of the Deprotonation of Carboxylic Acid by the Neighboring Amide NH Groups. *Bull. Chem. Soc. Jpn.* **2004**, *77*, 321−329.
(97) Tao, Y.; Zou, W.; Kraka, E. Strengthening of Hydrogen Bonding with the Push-Pull Effect. *Chem. Phys. Lett.* **2017**, *685*, 251−258.
(98) Pacios, L. F.; Gálvez, O.; Gómez, P. C. Variation of Geometries and Electron Properties along Proton Transfer in Strong Hydrogen-Bond Complexes. *J. Chem. Phys.* **2005**, *122*, No. 214307.
(99) Sánchez-Coronilla, A.; Balón, M.; Marcos, E. S.; Muñoz, M. A.; Carmona, C. A Theoretical Study of the Hydrogen Bond Donor Capability and Co-Operative Effects in the Hydrogen Bond Complexes of the Diaza-Aromatic Betacarbolines. *Phys. Chem. Chem. Phys.* **2010**, *12*, 5276−5284.
(100) Verma, A. K.; Modak, P.; Stixrude, L. New High-Pressure Phases in MOOH (M = Al, Ga, In). *Am. Mineral.* **2018**, *103*, 1906−1917.
(101) Tolborg, K.; Jørgensen, M. R. V.; Sist, M.; Mamakhel, A.; Overgaard, J.; Iversen, B. B. Low-Barrier Hydrogen Bonds in Negative Thermal Expansion Material H3[Co(CN)6]. *Chem. − Eur. J.* **2019**, *25*, 6814−6822.
(102) Escorcia, A. M.; Molina, D.; Daza, M. C.; Doerr, M. Acetylation of (R,S)-Propranolol Catalyzed by *Candida antarctica* Lipase B: An Experimental and Computational Study. *J. Mol. Catal. B: Enzym.* **2013**, *98*, 21−29.
(103) Kilgore, H. R.; Raines, R. T. N→π* Interactions Modulate the Properties of Cysteine Residues and Disulfide Bonds in Proteins. *J. Am. Chem. Soc.* **2018**, *140*, 17606−17611.
(104) Hoang, H. N.; Wu, C.; Hill, T. A.; Dantas de Araujo, A.; Bernhardt, P. V.; Liu, L.; Fairlie, D. P. A Novel Long-Range n to Π* Interaction Secures the Smallest Known A-Helix in Water. *Angew. Chem.* **2019**, *131*, 19049−19053.
(105) Wenzell, N. A.; Ganguly, H. K.; Pandey, A. K.; Bhatt, M. R.; Yap, G. P. A.; Zondlo, N. J. Electronic and Steric Control of N→π* Interactions: Stabilization of the α-Helix Conformation without a Hydrogen Bond. *ChemBioChem* **2019**, *20*, 963−967.
(106) Newberry, R. W.; VanVeller, B.; Guzei, I. A.; Raines, R. T. N→π* Interactions of Amides and Thioamides: Implications for Protein Stability. *J. Am. Chem. Soc.* **2013**, *135*, 7843−7846.
(107) Newberry, R. W.; Bartlett, G. J.; VanVeller, B.; Woolfson, D. N.; Raines, R. T. Signatures of N→π* Interactions in Proteins. *Protein Sci.* **2014**, *23*, 284−288.
(108) Khatri, B.; Majumder, P.; Nagesh, J.; Penmatsa, A.; Chatterjee, J. Increasing Protein Stability by Engineering the n → Π* Interaction at the β-Turn. *Chem. Sci.* **2020**, *11*, 9480−9487.
(109) Windsor, I. W.; Gold, B.; Raines, R. T. An N→π* Interaction in the Bound Substrate of Aspartic Proteases Replicates the Oxyanion Hole. *ACS Catal.* **2019**, *9*, 1464−1471.
(110) Gorske, B. C.; Bastian, B. L.; Geske, G. D.; Blackwell, H. E. Local and Tunable N→π* Interactions Regulate Amide Isomerism in the Peptoid Backbone. *J. Am. Chem. Soc.* **2007**, *129*, 8928−8929.
(111) Gorske, B. C.; Stringer, J. R.; Bastian, B. L.; Fowler, S. A.; Blackwell, H. E. New Strategies for the Design of Folded Peptoids Revealed by a Survey of Noncovalent Interactions in Model Systems. *J. Am. Chem. Soc.* **2009**, *131*, 16555−16567.
(112) Choudhary, A.; Kamer, K. J.; Powner, M. W.; Sutherland, J. D.; Raines, R. T. A Stereoelectronic Effect in Prebiotic Nucleotide Synthesis. *ACS Chem. Biol.* **2010**, *5*, 655−657.
(113) Bürgi, H. B.; Dunitz, J. D.; Lehn, J. M.; Wipff, G. Stereochemistry of Reaction Paths at Carbonyl Centres. *Tetrahedron* **1974**, *30*, 1563−1572.
(114) Choudhary, A.; Kamer, K. J.; Raines, R. T. An N→π* Interaction in Aspirin: Implications for Structure and Reactivity. *J. Org. Chem.* **2011**, *76*, 7933−7937.
(115) Feliciano, M. A. M.; Gold, B. Unique, yet Typical Oxyanion Holes in Aspartic Proteases. *ACS Catal.* **2020**, *10*, 14201−14209.

https://doi.org/10.1021/acsomega.1c02559
ACS Omega 2021, 6, 20992−21004